Smart Rock Technology for Real-time Monitoring of Bridge Scour and Riprap Effectiveness – Design Guidelines and Visualization Tools (Progress Report No. 1)

Contract No: OASRTRS-14-H-MST
(Missouri University of Science and Technology)

Reporting Period: October 1 – December 31, 2014

PI: Genda Chen

Program Manager: Mr. Caesar Singh

Submission Date: January 20, 2015

TABLE OF CONTENTS

EXECUTIVE SUMMARY

In the first quarter of this project, bridge and river data collection began for the design of smart rocks and for the development of design guidelines. Three criteria from HEC18 and HEC23 were considered to evaluate the critical velocity of water flow for the incipient motion of cohesionless deposits, the critical shear stress of cohesionless deposits, and rock size in riprap design.

The localization algorithm of passive smart rocks was further studied and validated at an open field and at the Gasconade River Bridge site. The total magnetic field at any site is significantly affected by the orientation of a permanent magnet. In order to simplify the localization process and improve the localization accuracy, an Automatically Pointing to South System (APSS) was designed and prototyped as key part of a passive smart rock to automatically orient the magnet along the geographically south direction. Its performance was compared with that of the Arbitrarily Oriented Magnet (AOM).

The total magnetic field around a bridge site is affected by a permanent magnet, the Earth, and any other ferromagnetic substances. It is dominated by the effects of the Earth and other substances. The field intensity by the magnet is relatively small. To enable the localization of smart rocks, the small field intensity of the magnet or the combined field intensity of the Earth and other ferromagnetic substances must be evaluated accurately. In this report, the combined effect of the Earth and other substances is referred to as the ambient magnetic field. To enable the accurate measurements, an Ambient Magnetic Field Orientation Device (AMFOD) was designed and prototyped to determine inclination and declination angles of the ambient magnetic field at various measurement points. At the bridge site, both spatial and temporal changes of the ambient magnetic field ought to be taken into account.

I - TECHNICAL STATUS

I.1 ACCOMPLISHMENTS BY MILESTONE

In this quarter, measurements were taken from field testing of passive smart rocks and data was analyzed to understand the effect of environmental ferrosubstances (e.g. rebar in bridge) on the magnetic field measurement at bridge site and evaluate the accuracy of localization identification results. For smart rock design, initial preparations began to collect necessary data for the evaluation of three criteria in terms of critical velocity of water flow, critical shear stress of a rock in riverbed, and riprap sizing.

Task 1.1 Motion of Smart Rocks under Various Flow Conditions - Critical Flow Conditions Summarized for Various Cases

In this quarter, bridge and river data are being collected to determine the critical velocity of water flow for incipient motion of cohesionless particles and the critical shear stress of cohesionless particles, following the guidelines in HEC18 and HEC23.

Task 1.2 Design Guidelines of Smart Rocks - Draft Design Guidelines Completed & Sent out for Review

There is no activity in this quarter.

Task 2.1 Final Design of Smart Rocks - CAD Drawings Completed

The localization algorithm proposed previously was validated at an open field (Ber Juan Park) and at a bridge site (Gasconade River Bridge, US Hwy63). The magnetic field of a permanent magnet in smart rocks is contaminated by the significant magnetic fields of the Earth and any nearby ferromagnetic substances such as rebar in concrete members of a bridge and washed-by metals in the river. To separate the magnet's effect from the combined magnetic field measurement, dominated by the effect of the Earth and the substances, the ambient magnetic field (from a combined effect of the Earth and other ferromagnetic substances) must be evaluated accurately and updated over time. To this endeavor, a special device is designed in this study and applied to take baseline data before and after a flood event even at the same location since the Earth's magnetic poles move around and the washed-by metals in the rive change over time. The Earth's magnetic field is generated by the swirling motions of molten metal in Earth's outer core. Those swirling motions are changing all the time. For example, the poles moved about 9 km (5.6 miles) per year in the first part of the 20th century, and about 41 km (25 miles) per year in recent years.

A. Approximate Solution of the Total Magnetic Field of a Cylindrical Permanent Magnet and Ambient Ferromagnetic Substances in Absolute XYZ Coordinate System

As illustrated in Figure 1, consider an absolute XYZ Cartesian coordinate system with X, Y, and Z axis pointing west, south and up on the ground surface. The origin of the XYZ system is a

reference point near the project site. The ambient magnetic field at the measurement station, Point Q(X, Y, Z) in Figure 1, is represented by a vector $\mathbf{B}_A$, which is determined by a magnetic intensity B_A and two angles, θ and φ. The parameter φ in [0, 2π] is the angle spanned from the X axis to the projected vector of the ambient magnetic field vector $\mathbf{B}_A$ in XOY plane and the parameter θ in [0, π] represents the angle spanned from the projected vector to $\mathbf{B}_A$. Therefore, the three components (B_{XA}, B_{YA}, B_{ZA}) of the ambient magnetic field along X-, Y-, and Z-directions are:

$$B_{XA} = B_A \cos\theta \cos\varphi \tag{1a}$$

$$B_{YA} = B_A \cos\theta \sin\varphi \tag{1b}$$

$$B_{ZA} = B_A \sin\theta \tag{1c}$$

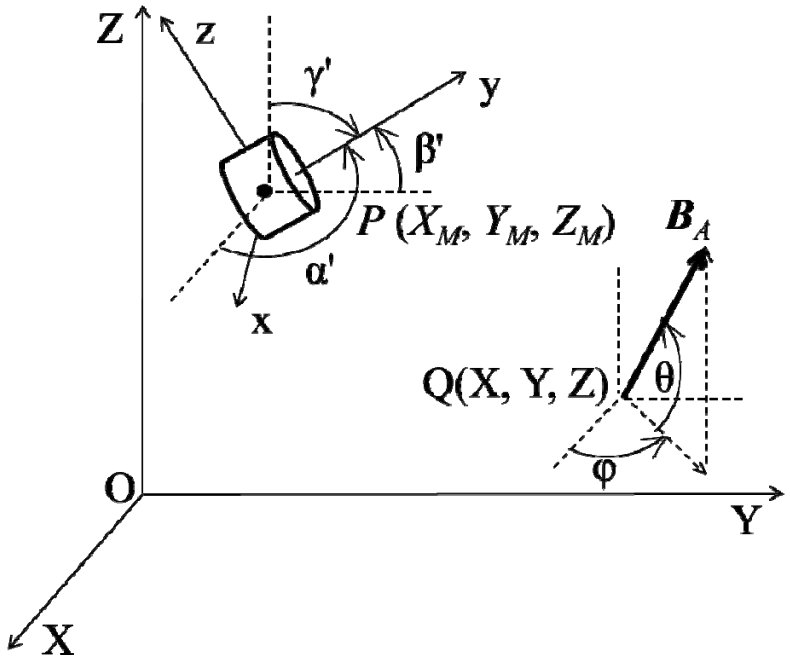

Figure 1 The Absolute XYZ Coordinate System, Local xyz Coordinate System of a Permanent Magnet P, and Ambient Magnetic Field Vector at a Measurement Station Q

The centroid of a permanent magnet is positioned at Point P(X_M, Y_M, Z_M) in the XYZ coordinate system. The orientation of the magnet is defined by a local xyz coordinate system. The xyz system would be formed if the XYZ system were to rotate first about X-axis by α, then about Y-axis by β, and finally about Z-axis by γ. The xyz can also be defined by the cosine directions of y-axis (cosα', cosβ', cosγ') and z-axis (cosα", cosβ", cosγ") in the XYZ system. Once y- and z-axis are fixed, the x-axis can take the direction perpendicular to the yoz plane following the right hand rule. The relation between (α', β', γ') as illustrated in Figure 1 and (α, β, γ) can be derived as:

$$\cos\alpha' = -\cos\beta \sin\gamma \tag{2a}$$

$$\cos\beta' = -\sin\alpha \sin\beta \sin\gamma + \cos\alpha \cos\gamma \tag{2b}$$

$$\cos\gamma' = \cos\alpha \sin\beta \sin\gamma + \sin\alpha \cos\gamma \tag{2c}$$

Similarly, the relation between (α", β", γ") and (α, β, γ) can be expressed into:

$$\cos\alpha'' = \sin\beta \tag{3a}$$
$$\cos\beta'' = -\sin\alpha\cos\beta \tag{3b}$$
$$\cos\gamma'' = \cos\alpha\cos\beta \tag{3c}$$

The total magnetic field intensity at the origin from the permanent magnet and the ambient magnetic field can be expressed into:

$$B = \sqrt{(B_{XM} + B_{XA})^2 + (B_{YM} + B_{YA})^2 + (B_{ZM} + B_{ZA})^2} \tag{4}$$

in which (B_{XM}, B_{YM}, B_{ZM}) represents three components of the magnetic field vector $\mathbf{B}_M$ of the permanent magnet. Specifically, the three components can be expressed into:

$$\begin{pmatrix} B_{XM} \\ B_{YM} \\ B_{ZM} \end{pmatrix} = \mathbf{T}^{-1} \begin{pmatrix} k3xy / r^5 \\ k(2y^2 - x^2 - z^2) / r^5 \\ k3zy / r^5 \end{pmatrix} \tag{5}$$

Where $k = \mu_0\mu/4\pi$ is a constant of the permanent magnet (e.g. k=10^{-9}Nm^2/A), μ_0 is the permeability of vacuum in N/m^2, μ is the magnetic moment in Am^2, $r = \sqrt{x^2 + y^2 + z^2}$, $x = a_{xX}(X - X_M) + a_{xY}(Y - Y_M) + a_{xZ}(Z - Z_M)$, $y = a_{yX}(X - X_M) + a_{yY}(Y - Y_M) + a_{yZ}(Z - Z_M)$, $z = a_{zX}(X - X_M) + a_{zY}(Y - Y_M) + a_{zZ}(Z - Z_M)$, and

$$\mathbf{T} = \begin{bmatrix} a_{xX} & a_{xY} & a_{xZ} \\ a_{yX} & a_{yY} & a_{yZ} \\ a_{zX} & a_{zY} & a_{zZ} \end{bmatrix} = \begin{bmatrix} \cos\beta\cos\gamma & \cos\beta\sin\gamma & -\sin\beta \\ \sin\alpha\sin\beta\cos\gamma - \cos\alpha\sin\gamma & \sin\alpha\sin\beta\sin\gamma + \cos\alpha\cos\gamma & \sin\alpha\cos\beta \\ \cos\alpha\sin\beta\cos\gamma + \sin\alpha\sin\gamma & \cos\alpha\sin\beta\sin\gamma - \sin\alpha\cos\gamma & \cos\alpha\cos\beta \end{bmatrix}.$$

Overall, the total magnetic intensity B in Eq. (4) at any point (X, Y, Z) depends upon the ambient magnetic field intensity B_A, the θ and φ angles of the ambient magnetic field, the coefficient k of the magnet, the location (X_M, Y_M, Z_M) and orientation (α, β, γ) of the magnet. That is, B = B (B_A, θ, φ, k, X_M, Y_M, Z_M, α, β, γ, X, Y, Z). Given k , θ , φ and B_A at each measurement point (X, Y, Z) of a project site, the total magnetic field intensity of the ambient and magnet B is a function of (X_M, Y_M, Z_M) and (α, β, γ). To accurately determine the location and orientation of a magnet from measured total intensities, measurements must be taken at a minimum of six stations in practical applications.

B. Magnet Localization Algorithms

B.1 Unknown Orientation

Assume that measurements $B_i^{(M)}$ are taken at n stations around a bridge pier (X_i, Y_i, and Z_i, i=1, 2, …, n). At each station, the theoretically predicted intensity $B_i^{(P)}$ can be calculated from Eq. (4) when X = X_i, Y = Y_i, and Z = Z_i. Therefore, the square-root-of-the-sum-of-the-squared (SRSS) error between the predicted intensity $B_i^{(P)}$ and the measured intensity $B_i^{(M)}$, $J(X_M, Y_M, Z_M, \alpha, \beta, \gamma)$, can be evaluated by:

$$J(X_M, Y_M, Z_M, \alpha, \beta, \gamma) = \sqrt{\sum_{i=1}^{n} [B_i^{(P)} - B_i^{(M)}]^2} \tag{6}$$

To minimize the SRSS error, the following six partial differential equations must be satisfied:

$$\frac{\partial J(X_M, Y_M, Z_M, \alpha, \beta, \gamma)}{\partial X_M} = 0 \tag{7a}$$

$$\frac{\partial J(X_M, Y_M, Z_M, \alpha, \beta, \gamma)}{\partial Y_M} = 0 \tag{7b}$$

$$\frac{\partial J(X_M, Y_M, Z_M, \alpha, \beta, \gamma)}{\partial Z_M} = 0 \tag{7c}$$

$$\frac{\partial J(X_M, Y_M, Z_M, \alpha, \beta, \gamma)}{\partial \alpha} = 0 \tag{7d}$$

$$\frac{\partial J(X_M, Y_M, Z_M, \alpha, \beta, \gamma)}{\partial \beta} = 0 \tag{7e}$$

$$\frac{\partial J(X_M, Y_M, Z_M, \alpha, \beta, \gamma)}{\partial \gamma} = 0 \tag{7f}$$

from which both the coordinate (X_M, Y_M, Z_M) and orientation (α, β, γ) of a permanent magnet can be determined. Note that the orientations are defined in a relative sense with respect to the Earth's geographical south.

B.2 Known Orientation (α=0, β=0, and γ=0)

In this case, the SRSS error in Eq. (6) is simplified into $J(X_M, Y_M, Z_M)$ and the xyz coordinate system is identical to the XYZ coordinate system. As such, only the first three equations in (7) are required to derive a solution for a minimum error. For clarity, the three partial differential equations are re-written in Eq. (8) as:

$$\frac{\partial J(X_M, Y_M, Z_M)}{\partial X_M} = 0 \tag{8a}$$

$$\frac{\partial J(X_M, Y_M, Z_M)}{\partial Y_M} = 0 \tag{8b}$$

$$\frac{\partial J(X_M, Y_M, Z_M)}{\partial Z_M} = 0 \tag{8c}$$

C. Experimental Validation of the Magnet Localization Algorithm at Bridge Site

In this section, one smart rock with known orientation referred to as Automatically Pointing to South System (APSS) and another smart rock with unknown orientation referred to as Arbitrarily Oriented System (AOS) are tested at the Gasconade River Bridge site to validate the localization algorithms in Eqs. (7) and (8).

C.1 Evaluation of k, B_A, θ and φ

The coefficient k was first evaluated at an open field (Ber Juan Park, Rolla, MO) before the smart rocks were tested at the bridge site. For APSS and AOS, k = 42542.27($nT \cdot m^3$) and 41890.13($nT \cdot m^3$), respectively.

At the bridge site, the ambient magnetic field lines are no longer in parallel due to the combined effect of the Earth and other ferromagnetic substances, such as reinforcement in bridge piers and deck. The ambient magnetic field varies in space and can be uniquely defined by three parameters (B_A, θ and φ) at each measurement points. To evaluate these parameters, an Ambient Magnetic Field Orientation Device (AMFOD) was developed and prototyped to measure the angles θ and φ at each measurement point in addition to a magnetometer for field intensity measurement.

C.2 Test Setup and Procedures

All tests were conducted near the bridge pier as shown in Figure 2. The bridge pier experienced foundation scour from previous flood events. The test layout is shown in Figure 3. Three locations of each of two smart rocks (APSS and AOS), designed by M1, M2 and M3 in Figure 3(a), were selected to take into account a combination of horizontal positions and depths in bridge scour monitoring. M1, M2, M3 were well spaced as clearly shown in Figure 3(a) in horizontal plane. M3 was placed in the scour hole. To locate each smart rock, a total of 34 measurement points with a G858 Magnetometer (P1 to P34, marked by 34 wooden and plastic poles during actual tests), were selected around M1, M2, and M3. The sensor head was placed on top of every wooden or plastic pole to measure the ambient and total magnetic intensities for each smart rock location. A total station was used to survey the coordinates of three smart rocks' locations and 34 sensor positions as ground true data. A prism was placed at the same location of the sensor head on top of the wooden poles to ensure that the magnetic field intensity and the coordinates are collocated. In addition, the AMFOD was set at the 34 points to measure the angles of θ and φ before the smart rocks were deployed at each location.

Figure 2 The Bridge Pier with a Scour Hole

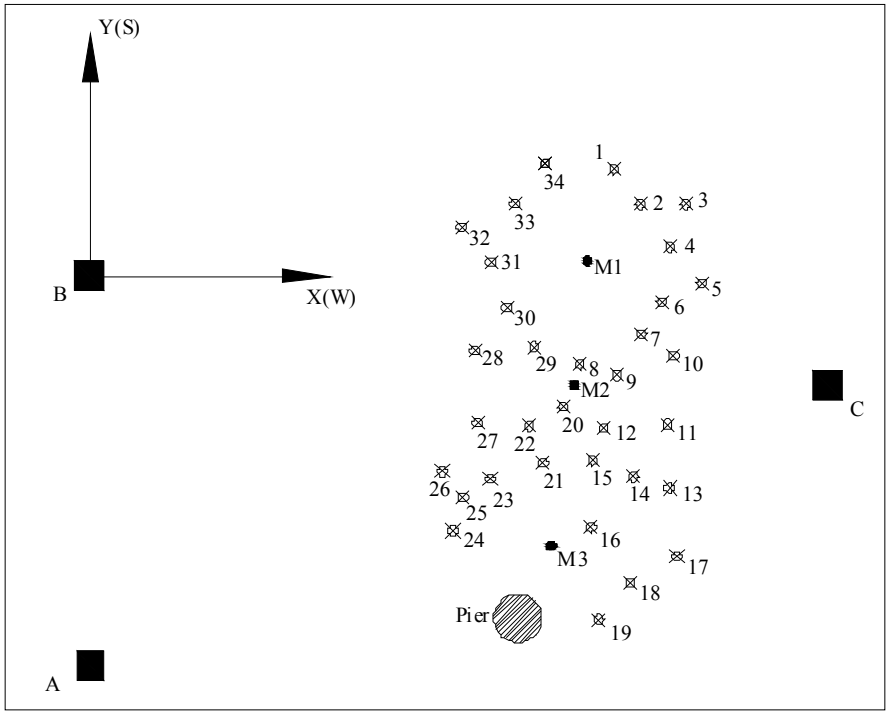

(a) Schematic view of smart rock and sensor locations in plane

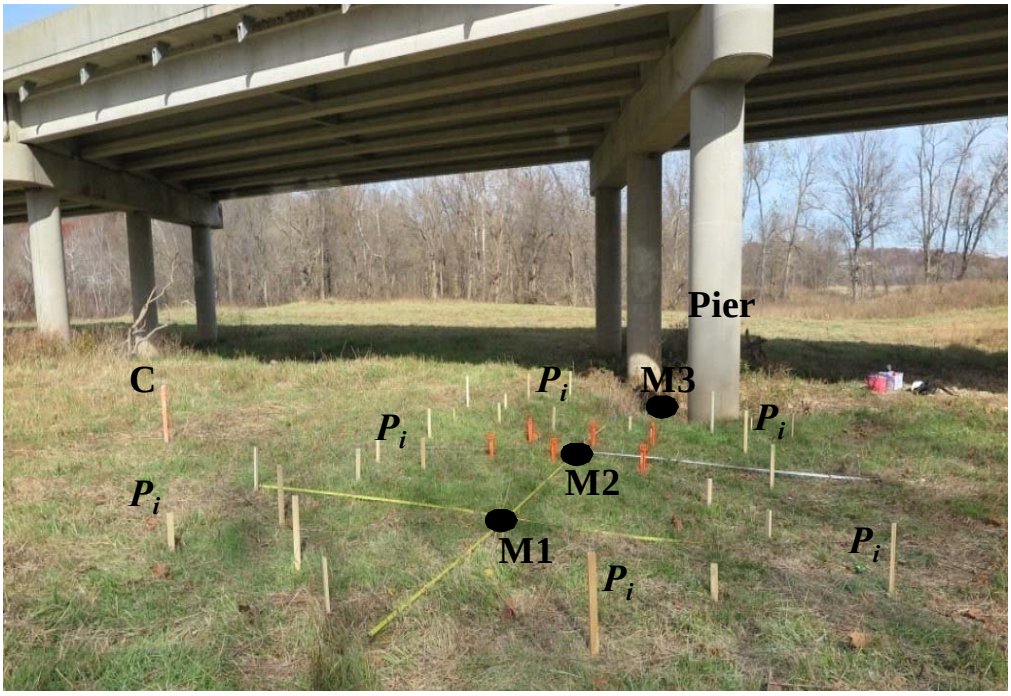

(b) Layout of smart rocks and sensor head

Figure 3 Test Setup at Bridge Site

For a systematic study, a step-by-step test procedure was developed and implemented at the bridge site. It is detailed as follows:

(1) ***Set the XYZ Coordinate System***. As shown in Figure 3(a), a point A marked by a wooden pole was selected far away from the bridge pier to avoid potential measurement interference by ferromagnetic substances of the bridge pier. Place a high-precision military compass on the wooden pole to survey the geographical South direction, select a point B on the line of the south direction, and check that all of the measurement points were in the sight of point B. Select point B as the origin and the direction from A to B as the Y-axis. The X-axis is thus selected pointing to West and the Z-axis is perpendicular to the XOY plane or out of the paper as shown in Figure 3(a).

(2) ***Select the Locations of Smart Rocks and Sensor Head***. As shown in Figures 3(a, b), the smart rocks were located from far away to close to the bridge pier in order to understand the variation of the ambient magnetic field, the angles, and the total magnetic field. Smart rock locations, M1, M2 and M3, were marked by inserting bottle caps into the ground for easy placement of smart rocks on the ground and convenient collection of coordinates. The 34 wooden poles, P1 to P34, were distributed around the M1, M2 and M3 and bounded between the circles with diameter of 1.5m and 5m in order to avoid the dead zone of the magnetometer at each location of smart rocks. Three measurement tapes crossed at M1 and M2 were displayed to assist in the estimation of distance between a smart rock and the sensor head.

(3) ***Select a Calibration Point C for AMFOD***. A fixed object is needed to assist in the final determination of angle φ. As such, Point C indicted in Figures 3(a, b) marked by a tall wooden pole was selected out of the range of 34 measurement points. The selection of Point C was to ensure that the light from the horizontal laser pointer2 can reach the wooden pole at Point C when the AMFOD was stationed at each sensor point.

(4) ***Determine the Coordinates of Smart Rocks, Sensor Head and Calibration Point***. A total station was used to survey the coordinates of various points at the test site. Throughout the tests, one person operated the total station and another person held one prism as seen in Figure 4 to ensure the consistent accuracy of coordinate measurements. For each survey, the bottom center of the prism was aligned with the center of the top of the wooden pole and bottle caps since the magnetic field intensity is pretty sensitive to Z-coordinate.

Figure 4 Total Station and Prism for Positioning

(5) ***Measure θ and φ***. As shown in Figure 5, the AMFOD was placed at one measurement point by aligning the center of its tripod to the top center of the plastic pole, in which the center of the high-precision APSS should be kept along the extension line of the plastic pole by adjusting the tripod with the high precision bubble level attached on the horizontal disk of the AMFOD. At each measurement point, the tripod was first adjusted horizontally without presence of the high-precision APSS. That is, after the horizontal Laser 2 was switched on, the tripod was rotated until the shooting light hit on the wooden pole at Point C and immediately locked at that position. The high-precision APSS was then put back to the tapered support. After the inside ball with a magnet was automatically aligned to the ambient magnetic field in several seconds, Laser 1 was switched on and its supporting ring was manually turned vertically, in combination with horizontal adjustment by the tunable disk, to facilitate the light going through the hole at the center line of the high-precision APSS and hit on the center of the laser acceptor. Finally, the two lasers were switched off and the two angles θ and φ can be read from the digital marks on the vertical ring and horizontal disk, respectively. The above process was repeated for all 34 points.

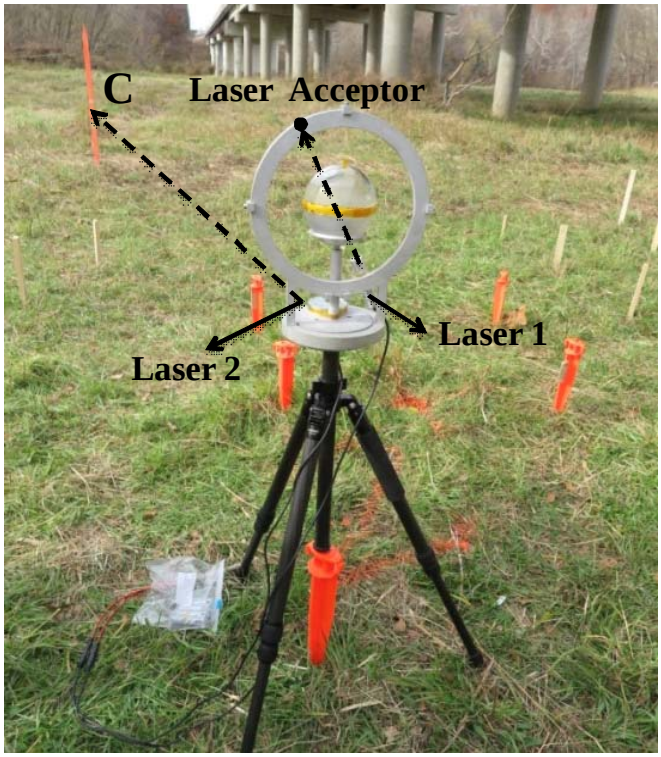

Figure 5 AMFOD Setup and Operational Mechanism

(6) ***Measure the Ambient Magnetic Field Intensity***. One sensor head of the magnetometer was faced on the ground and ensured to be perpendicular to the ground by a bubble level attached onto the sensor head as shown in Figure 6. It is noted that a 57.7cm wooden stick fastened onto the sensor head was to keep the center of the sensor head the same location at the center of the high-precision APSS in the AMFOD so that the magnetometer and the AMFOD provided the corresponding magnitude and direction of the ambient magnetic field vector, respectively. In addition, measurements should be made when there are no vehicles on the bridge deck to avoid any potential interference. At each point, at least three measurements were taken to ensure accuracy and repeatability.

Figure 6 Magnetometer Setup and Operation

(7) ***Measure the Total Magnetic Field Intensity of APSS at M1, M2 and M3***. The APSS smart rock was placed at each point M1, M2 or M3 as seen in the Figure 7. The center of the magnet was aligned with the center of the bottle cap at each point. The total magnetic field was generated by the magnet and the ambient magnetic field. The same setup of the magnetometer stated in step 6 was applied and repeated to measure the total magnetic field intensity for the APSS at M1, M2 and M3, respectively.

(a) $M1_{APSS}$ or $M2_{APSS}$ (b) APSS at M3

Figure 7 APSS Deployment

(8) ***Measure the Total Magnetic Field Intensity of AOS at M1, M2 and M3***. In this final step, the AOS was placed at point M1, M2 and M3 as shown in Figure 8. The center of the plastic box with the centered magnet was kept in alignment with the center of the bottle cap at each point. The same setup of the magnetometer stated in step 6 was applied and repeated to measure the total magnetic field intensity for all the AOS at M1, M2 and M3.

(a) $M1_{AOS}$ or $M2_{AOS}$ (b) AOS at M3

Figure 8 AOS Deployment

C.3 Test Results and Discussion

Ambient Magnetic Field Intensity in XYZ Coordinate System The θ angle can be directly read from the digital marks on the vertical ring of the AMFOD. However, the φ angle must be transformed from the directly measured angle φ' read from the digital marks on the horizontal disk of the AMFOD and the φ_0 angle from the test setup in XYZ coordinate system. As shown in Figure 9, $\boldsymbol{B}_A^{Pi}$ denotes the ambient magnetic field vector at measurement point P_i in XOY plane, P_iC represents the light of Laser 2 shooting to the wooden pole at Point C, the local coordinate P_i-xoy is parallel to the global coordinate of XOY, and φ' in [0,π] is the angle spanned from the extension of vector $-\boldsymbol{B}_A^{Pi}$ to the line P_iC in counterclockwise. Therefore, the direction of the ambient magnetic field φ in [0, 2π] in XOY plane is equal to $2\pi-\varphi'+\varphi_0$, where φ_0 in [0,2π] is the angle between line P_iC and X-axis in counterclockwise and equal to $\arctan[(Y_C-Y_{Pi})/(X_C-X_{Pi})]$.

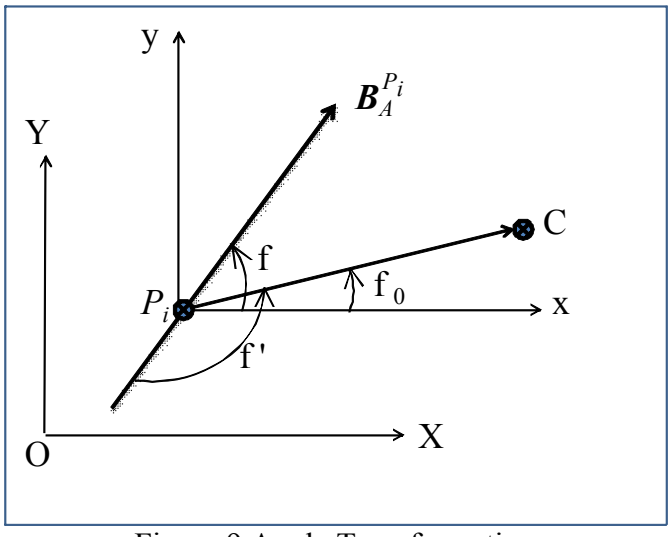

Figure 9 Angle Transformation

Table 1 summarizes the coordinates of 34 sensor locations in the XYZ coordinate system, the direction of the ambient magnetic field vector, and the ambient magnetic field intensities at each measurement point.

Table 1 Sensor Coordinates and Ambient Magnetic Field Intensities

Measurement Point	Sensor Coordinates			Ambient Magnetic Field Direction		Ambient Magnetic Field Intensity			
	***X*/m**	***Y*/m**	***Z*/m**	**θ / rad**	**φ / rad**	**B_A /nT**	**B_{AX} /nT**	**B_{AY} /nT**	**B_{AZ} /nT**
C	15.284	-2.264	N/A	N/A	N/A	N/A	N/A	N/A	N/A
P1	10.882	2.202	-0.547	1.213	1.503	50798	1213	17748	47581
P2	11.425	1.481	-0.454	1.222	1.525	51417	810	17567	48316
P3	12.365	1.479	-0.576	1.222	1.477	51363	1637	17491	48266
P4	12.040	0.587	-0.483	1.197	1.485	51366	1603	18674	47825
P5	12.701	-0.160	-0.512	1.196	1.512	51296	1102	18768	47727
P6	11.868	-0.544	-0.585	1.190	1.450	51356	2299	18933	47684
P7	11.452	-1.211	-0.607	1.178	1.294	51473	5387	18947	47555
P8	10.174	-1.840	-0.707	1.152	1.275	51952	6159	20213	47460
P9	10.940	-2.065	-0.717	1.143	1.372	51790	4252	21052	47127
P10	12.119	-1.657	-0.695	1.148	1.338	51354	4862	20482	46841
P11	11.991	-3.082	-0.618	1.131	1.423	51692	3236	21770	46772
P12	10.670	-3.162	-0.730	1.127	1.496	52556	1685	22480	47476
P13	12.031	-4.399	-0.795	1.126	1.356	52052	4782	21893	46982
P14	11.284	-4.169	-0.698	1.122	1.286	52735	6432	21946	47518
P15	10.436	-3.832	-0.696	1.112	1.377	53369	4545	23205	47845
P16	11.403	-5.217	-0.720	1.161	1.340	53320	4867	20697	48898
P17	12.185	-5.815	-0.536	1.140	1.307	52404	5710	21140	47610
P18	11.217	-6.364	-0.559	1.148	1.135	54141	9368	20119	49383
P19	10.568	-7.123	-0.598	1.155	1.132	55922	9588	20429	51166
P20	9.822	-2.717	-0.695	1.141	1.277	52728	6367	21006	47942
P21	9.413	-3.877	-0.808	1.126	1.286	54619	6616	22564	49299
P22	9.122	-3.115	-0.753	1.121	0.940	53573	13751	18830	48232
P23	8.313	-4.215	-0.561	1.114	1.331	55654	5848	23866	49936
P24	7.536	-5.287	-0.701	1.103	1.599	59033	-750	26606	52692
P25	7.750	-4.591	-0.918	1.096	1.530	57317	1068	26178	50979
P26	7.315	-4.055	-0.786	1.127	1.410	55304	3805	23414	49958
P27	8.043	-3.046	-0.613	1.127	1.239	53573	7494	21723	48394
P28	7.989	-1.553	-0.689	1.143	1.327	52046	5210	20945	47360
P29	9.216	-1.476	-0.691	1.190	1.267	51939	5767	18406	48225
P30	8.651	-0.664	-0.787	1.189	1.299	51596	5164	18539	47873
P31	8.321	0.282	-0.762	1.159	1.426	51358	2962	20346	47062
P32	7.714	1.007	-0.628	1.141	1.460	51326	2370	21234	46668
P33	8.813	1.487	-0.724	1.143	1.511	51330	1262	21249	46709
P34	9.455	2.322	-0.436	1.162	1.410	51417	3264	20158	47188

APSS Localization Due to limited space, only the identified location of M1 is presented here. Specifically, Table 2 shows the measured coordinates and total field intensities ($B_i^{(M)}$) at 18 points when the APSS was located at M1, which was compared with the predicted location using the measured coordinates of sensor points. Overall, it can be observed from the test results at M1, M2, and M3 that the SRSS prediction error ranges from 8.5 to 18 cm, which is quite small in comparison with the diameter of smart rocks (approximately 30cm).

Table 2 Predicted and Measured Location of the APSS: $M1_{APSS}$

Location of Sensor Head	X(m)	Y(m)	Z(m)	$B_i^{(M)}$ (nT)
P1	10.882	2.202	-0.517	58120
P2	11.425	1.481	-0.424	56946
P3	12.365	1.479	-0.546	51808
P4	12.040	0.587	-0.453	49719
P5	12.701	-0.160	-0.482	49893
P6	11.868	-0.544	-0.555	47968
P7	11.452	-1.211	-0.577	49729
P8	10.174	-1.840	-0.677	52129
P9	10.940	-2.065	-0.687	52055
P10	12.119	-1.657	-0.665	50942
P20	9.822	-2.717	-0.665	53002
P28	7.989	-1.553	-0.659	51464
P29	9.216	-1.476	-0.661	51031
P30	8.651	-0.664	-0.757	48911
P31	8.321	0.282	-0.732	49487
P32	7.714	1.007	-0.598	51185
P33	8.813	1.487	-0.694	55240
P34	9.455	2.322	-0.406	56421
Predicted APSS Location $M1_{APSS}$	10.249	0.454	-1.352	N/A
Measured APSS Location $M1_{APSS}$	10.326	0.305	-1.407	
Location Prediction Error for M_{APSS}	-0.077	0.149	0.055	
SRSS Error in Coordinate	0.176 m			

AOS Localization Table 3 gives the measured coordinates (X, Y, Z) and total magnetic intensities ($B_i^{(M)}$) at 18 sensor points when the AOS is located at M1. Similar to the APSS case, The prediction location error of the magnet ranges from 9.3 to 15.4 cm. Once again, this range of errors is small compared with the size of smart rocks, demonstrating satisfactory accuracy in smart rock localization for bridge scour monitoring.

Table 3 Predicted and Measured Location of the AOS: $M1_{AOS}$

Location of Sensor Head	X(m)	Y(m)	Z(m)	$B_i^{(M)}$ (nT)
P1	10.882	2.202	-0.517	53558
P2	11.425	1.481	-0.424	52767
P3	12.365	1.479	-0.546	49746
P4	12.040	0.587	-0.453	47899
P5	12.701	-0.160	-0.482	48902
P6	11.868	-0.544	-0.555	45901
P7	11.452	-1.211	-0.577	46861
P8	10.174	-1.840	-0.677	48626
P9	10.940	-2.065	-0.687	49665
P10	12.119	-1.657	-0.665	49567
P20	9.822	-2.717	-0.665	51538
P28	7.989	-1.553	-0.659	50607
P29	9.216	-1.476	-0.661	48149
P30	8.651	-0.664	-0.757	47696
P31	8.321	0.282	-0.732	50501
P32	7.714	1.007	-0.598	51340
P33	8.813	1.487	-0.694	54907
P34	9.455	2.322	-0.406	54539
Predicted AOS Location $M1_{AOS}$	10.265	0.235	-1.456	N/A
Measured AOS Location $M1_{AOS}$	10.326	0.305	-1.422	
Location Prediction Error for $M1_{AOS}$	-0.061	-0.070	-0.034	
SRSS Error in Coordinate	0.099 m			

Tasks 2.2 Prototyping of Passive Smart Rocks - Concrete Encasement Cast

There is not activity in this quarter.

Task 3.1 Time- and Event-based Field Measurements - Field Tests Completed & Reported

This task will not start till the 3rd quarter.

Task 3.2 Visualization Tools for Rock Location Mapping over Time - Software Completed & Tested

This task will not start till the 5th quarter.

Task 4 Technology Transfer, Report and Travel Requirements - Quarterly Report Submitted, Travel Completed, or Meeting Conducted

The 1st quarterly report is being submitted. A kickoff meeting with Technical Advisory Council (TAC) was organized on November 14. The TAC consists of Dr. Kornel Kerenyi from Federal Highway Administration, Kevin Flora from California Department of Transportation, Dale Henderson from Missouri Department of Transportation, and Malcolm Hodge from SmartSensys. In addition, William Stone and Jennifer Harper also contributed to the discussion and provided valuable input at the project kickoff meeting.

I.2 PROBLEMS ENCOUNTERED

In this quarter, contact was made with the California Department of Transportation about the selection of a second bridge to be tested and about the bridge drawings requested. Once the bridge and the river data become available, the size of smart rocks can be finalized for each bridge site.

I.3 FUTURE PLAN

The following task and subtasks will be executed during the next quarter.

Task 1.1 Motion of Smart Rocks under Various Flow Conditions - Critical Flow Conditions Summarized for Various Cases

The critical velocity of water flow for incipient motion of cohesionless particles and the critical shear stress of cohesionless particles as well as the riprap size will be evaluated to determine the size of smart rocks for each bridge site.

Task 1.2 Design Guidelines of Smart Rocks - Draft Design Guidelines Completed & Sent out for Review

After analysis is conducted to determine the size of smart rocks in Subtask 1.1, the experience and procedure to size the smart rocks will be summarized for reference in future design.

Task 2.1 Final Design of Smart Rocks - CAD Drawings Completed

The size of smart rocks will be finalized and details will be provided in CAD drawings after additional field tests have been completed to understand the effect of refill in scour hole and the incipient motion of smart rocks.

Tasks 2.2 Prototyping of Passive Smart Rocks - Concrete Encasement Cast

Based on the final design of smart rocks, concrete encasement will be cast for field deployment.

Task 3.1 Time- and Event-based Field Measurements - Field Tests Completed & Reported

This task will not start till the 3rd quarter.

Task 3.2 Visualization Tools for Rock Location Mapping over Time - Software Completed & Tested

This task will not start till the 5th quarter.

Task 4 Technology Transfer, Report and Travel Requirements - Quarterly Report Submitted, Travel Completed, or Meeting Conducted

The 2nd quarterly report will be prepared and submitted. Towards the end of next quarter, the 2nd meeting with Technical Advisory Council (TAC) will be organized to discuss the progress in the first 6 months. Feedbacks will be sought and considered in the execution of future tasks.
.

II – BUSINESS STATUS

II.1 HOURS/EFFORT EXPENDED

The planned hours and the actual hours spent on this project are given and compared in Table 4. In the first quarter, the actual hours are less than the planned hours, leading to an actual cumulative hour of approximately 19% of the planned hours. The cumulative hours spent on various tasks by personnel are presented in Figure 10.

Table 4 Hours Spent on This Project

Quarter	Planned		Actual	
	Labor Hours	Cumulative	Labor Hours	Cumulative
1	945	945	176	176
2				
3				
4				
5				
6				
7				
8				

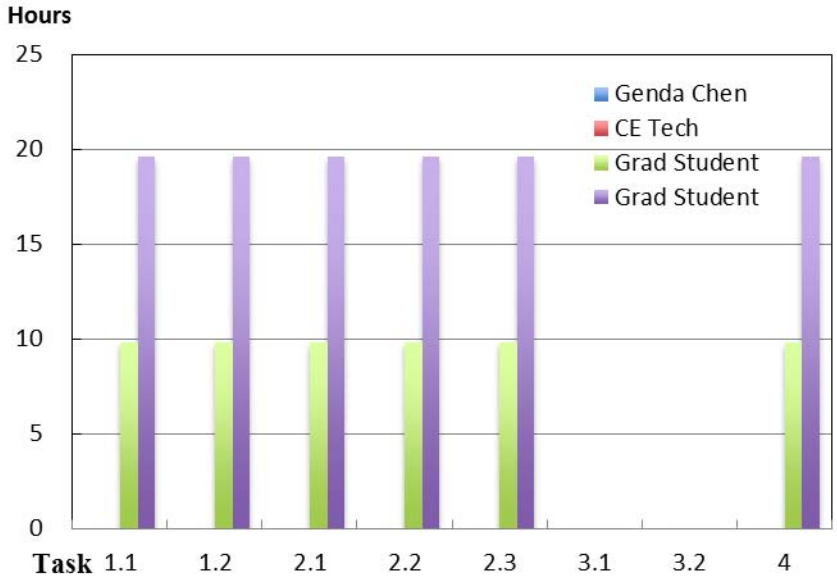

Figure 10 Cummulative Hours Spent on Various Tasks by Personnel

II.2 FUNDS EXPENDED AND COST SHARE

The budgeted and expended OST-R funds accumulated by quarter are compared in Figure 11. Approximately 33% of the budget has been spent till the end of first quarter. The actual cumulative expenditures from OST-R and MS&T/MoDOT are compared in Figure 12. The expenditure from OST-R is less than the combined amount from the MS&T and MoDOT.

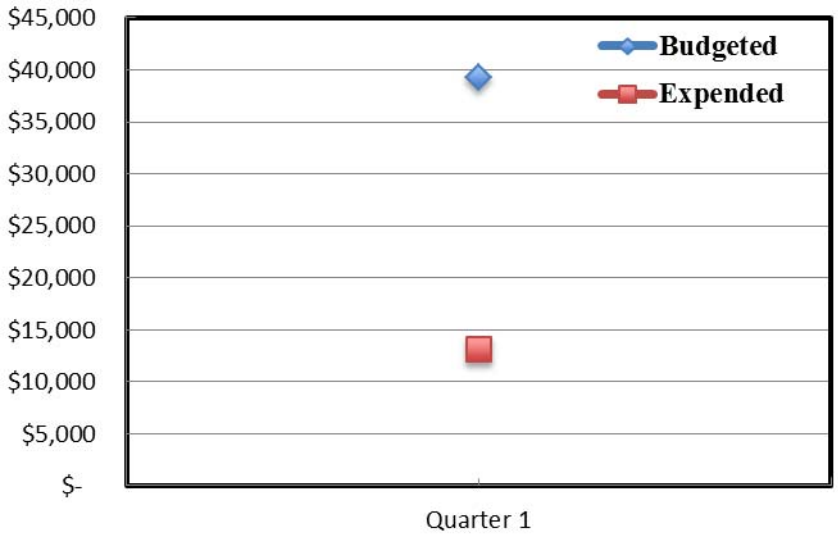

Figure 11 Comparison of OST-R Budget and Expenditure Accumulated by Quarter

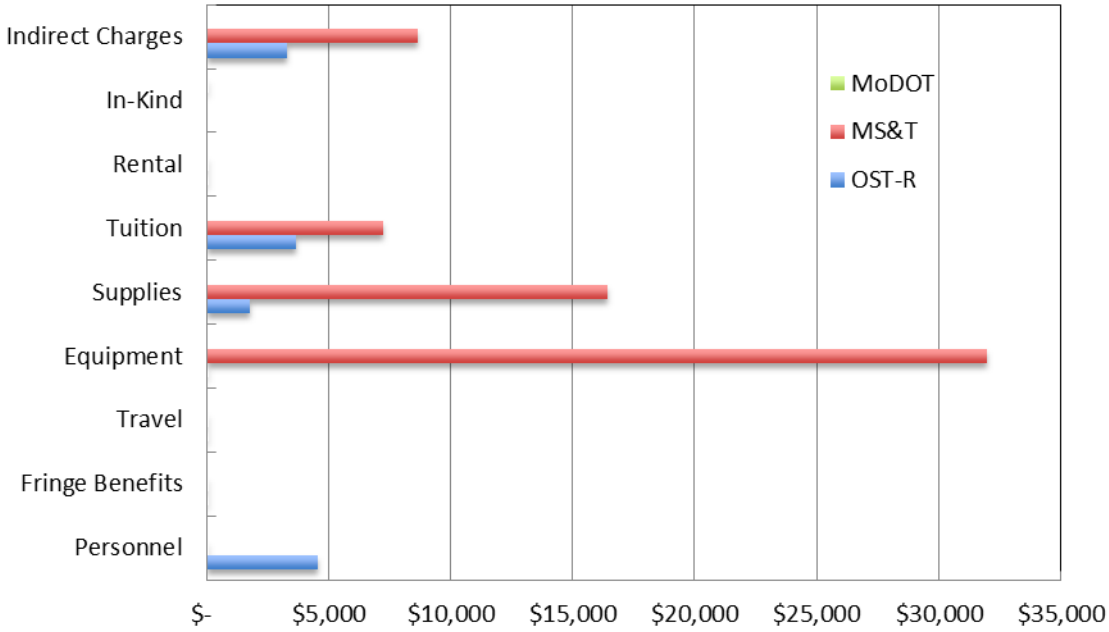

Figure 12 Cummulative Expenditures by Sponsor